U/Pb Zircon Geochronology and Tempo of the End-Permian Mass Extinction

S. A. Bowring,* D. H. Erwin, Y. G. Jin, M. W. Martin, K. Davidek, W. Wang

The mass extinction at the end of the Permian was the most profound in the history of life. Fundamental to understanding its cause is determining the tempo and duration of the extinction. Uranium/lead zircon data from Late Permian and Early Triassic rocks from south China place the Permian-Triassic boundary at 251.4 ± 0.3 million years ago. Biostratigraphic controls from strata intercalated with ash beds below the boundary indicate that the Changhsingian pulse of the end-Permian extinction, corresponding to the disappearance of about 85 percent of marine species, lasted less than 1 million years. At Meishan, a negative excursion in $\delta^{13}C$ at the boundary had a duration of 165,000 years or less, suggesting a catastrophic addition of light carbon.

The end of the Permian period marks the most widespread annihilation of life in the past 540 million years and the elimination of richly diverse marine communities dominated by the now-scarce brachiopods, bryozoans, and stalked echinoderms. Nearly 85% of marine species and some 70% of terrestrial vertebrate genera became extinct (*1*, *2*), and insects suffered their only mass extinction (*3*). The duration of this event has remained uncertain. Proposed extinction patterns include the following: (i) two separate extinctions, one in the Capitanian (late Middle Permian) and a second in the late Changhsingian (late Late Permian) (*4*–*6*); (ii) a long period of increased extinction beginning in the Capitanian and accelerating to a rapid pulse at the close of the Changhsingian (*2*, *7*); and (iii) a rapid extinction just at the close of the Changhsingian and perhaps extending into the earliest Triassic (*8*). Here, we provide U/Pb age determinations and stratigraphic information on taxon occurrences to discriminate among these patterns and to assess the possible causes of the extinction. Specifically using temporal constraints, we seek to determine a plausible chain of events that could explain the most profound extinction in the history of the planet.

Numerous Permian-Triassic (P-T) marine boundary sections are exposed in south China; these sections contain abundant interbedded volcanic ash beds. We sampled ash beds for U/Pb dating in the proposed P-T boundary stratotype at Meishan, Zhejiang Province, in early Late Permian–Early Triassic marine rocks near Heshan and Laibin in Guangxi Province (Fig. 1), and in the classic Guadalupian sections in Guadalupe Mountains National Park in Texas.

Permian-Triassic age estimates. The chronostratigraphic time scale for the Late Permian and Early Triassic is well established on the basis of conodont biozones, which are believed to be global and isochronous. The working definition for the base of the Triassic is marked by the first occurrence of the conodont *Hindeotus parvus* in the boundary section at Meishan (*9*). Here, paleontological and geochemical evidence indicates that the peak extinction was in the late Changhsingian Stage, the final stage of the Permian, and thus close to the P-T biostratigraphic boundary. At the Meishan section, an ash bed in quarry D (see below) immediately underlying the bed containing the paleontologically defined P-T boundary has been dated by Rb/Sr analysis of sanidine at 250 ± 6.0 million years ago (Ma) (*10*), by U/Pb super high-resolution ion microprobe (SHRIMP) analysis of zircons at 251.1 ± 3.4 Ma (*11*), and by $^{40}Ar/^{39}Ar$ dating of sanidine at 249.9 ± 1.5 Ma (*12*).

Recent estimates of the duration of the Wordian-Changhsingian stages have varied from 10 to 21 million years (My) (*13*). There are fewer estimates of the duration of the Changhsingian Stage, but the Late Permian (Wuchiapingian plus Changhsingian) is thought to have lasted between 5 and 16 My (*13*) on the basis of rock thickness, the number of conodont zones, and other approaches. A tuff within the *Pseudonodosaria borealis* zone of the Ingelara Formation of central Queensland, Australia, has provided a U/Pb SHRIMP date of 253.4 ± 3.2 Ma (*14*). Foraminifera from this zone suggest that it correlates with the Russian Kazanian (Wordian-Capitanian) sections (*15*), but the implied duration for the post-Kazanian interval is inconsistent with reported dates for the P-T boundary in south China.

In summary, the age of the P-T boundary is 250 to 251 Ma within the probable global stratotype section for the boundary. However, there are essentially no accurate constraints on the duration of the Late Permian.

Permian and Early Triassic stratigraphic sections. The classic P-T boundary section at Meishan is exposed in five closely spaced limestone quarries near Meishan, Changhsing, Zhejiang Province (Fig. 1). The series of abandoned quarries are labeled A, B, C, D, E, and Z from west to east, and quarry D serves as the type locality for the Changhsingian Stage and the Changhsing Formation (Fig. 2). We collected samples from six ash beds here. Sample MD96-7 is from bed 7, a 9-cm-thick greyish-yellow tuffaceous sandstone near the base of the Baoqing Member, the lower unit of the Changhsing Formation. Biostratigraphically, this unit is in the basal part of the *Clarkina subcarinata* conodont zone and about 7 m above the *C. orientalis* zone of the topmost Wuchiapingian Stage. Sample MZ96-(−4.3) was collected from quarry Z and is a silicified yellow- to buff-colored tuff that corresponds to bed 20. Sample MAW-b25 is the "boundary ash" at quarry A. This ash, previously considered to lie at the P-T boundary, actually occurs about 10 cm below the first occurrence of *H. parvus*. Lithologically, the ash bed is divided into a lower white clay (bed 25) and an upper black clay (bed 26), although bed 26 is not always present. Both are illite-montmorillonite

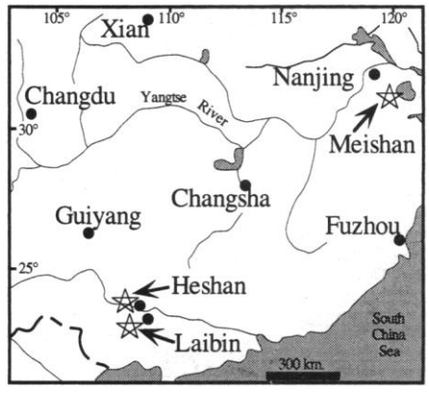

Fig. 1. Location map of the south China region showing sample location sites at Meishan, Heshan, and Laibin.

S. A. Bowring, M. W. Martin, and K. Davidek are in the Department of Earth, Atmospheric and Planetary Sciences, Massachusetts Institute of Technology, Cambridge, MA 02319, USA. D. H. Erwin is in the Department of Paleobiology, National Museum of Natural History, Washington, DC 20560, USA. Y. G. Jin and W. Wang are at the Laboratory of Paleobiology and Stratigraphy, Nanjing Institute of Geology and Paleontology, Academia Sinica, Nanjing, 210008, People's Republic of China.

*To whom correspondence should be addressed.

clay stones, but they contain different suites of fossils. We also sampled three ash beds within the Lower Triassic Chinglung Formation. These beds included a 9-cm-thick illite-montmorillonite clay at bed 28 [MZ96-(+0.17)], a 5-cm-thick yellowish illite-montmorillonite clay 225 cm above bed 25 at bed 33 (MDB96-33), and a 5-cm-thick greyish ash 670 cm above bed 25 and within bed 36 (MD96-293w), which is a rhythmically bedded bluish-grey calcareous mudrock containing the common bivalve *Claraia*.

The P-T boundary section at Matan lies near a small coal mine along the Hong Shui River, about 2 km from the town of Heshan, Guangxi Province (Fig. 1). The section exposed is the type section of the Talung Formation, the basinal sequence of the Changhsingian. The Talung Formation in Matan is 16 m thick and corresponds to the upper part of the Changhsing Formation. At Matan, a spectacular sequence of silicic pyroclastic rocks crops out just below the boundary. The pyroclastic deposits are bedded and consist of several upward fining sequences that vary from coarse crystal-rich deposits to fine clay stone. Here, we collected four different samples to test reproducibility (H-Matan96-1, -3, -6, and -7). Samples H-Matan96-6 and -7 are from immediately below the P-T boundary.

The P-T boundary section at Penglaitan is exposed along the banks of the Hong Shui River near the town of Laibin (Fig. 1). Here, a 9-m-thick, well-graded pyroclastic sequence crops out below the boundary in the river bottom. Specimens of the ammonoids *Rotodiscoceras* and *Pleuronodoceras* have recently been discovered beneath this unit, confirming a late Changhsingian age. The unit fines upward from a sandy crystal-rich base to a porcellanite top. Sample LP96-2 was collected near the top of the volcanic sequence.

Conodont biostratigraphy allows correlation among these three boundary sections in China. MD96-7 from Meishan is from the base of the Changhsingian, and LP96-2 and MZ96-(−4.3) are from the upper Changhsingian. The Heshan samples H-Matan96-1 and -3 are immediately below H-Matan96-6 and -7, which occur approximately at the P-T boundary, on either side of the river, and are thus correlative with MAW-b25 at Meishan. The P-T boundary must be older than beds MZ96-(+0.17) and MDB96-33 at Meishan.

An ash bed was also sampled in Texas, where it occurs between the Hegler and Pinery limestone members of the Bell Canyon Formation at Nipple Hill, Guadalupe Mountains National Park, Texas. The ash is 6 to 8 cm thick and lies 2 m above the top of the Hegler Member, within the undifferentiated Bell Canyon Formation, and 20 m below the base of the *Jinogondolella postserrata* conodont zone. This zone defines the base of the Capitanian substage of the Guadalupian Series. This stratigraphic interval is within the proposed type section for the Capitanian Stage (*16*). Thus, as in the south China sections, there are no correlation difficulties.

Uranium/lead zircon geochronology. With the U/Pb method applied to zircons separated from strata-bound volcanic layers, it is possible to use two independent decay schemes ($^{238}U/^{206}Pb$ and $^{235}U/^{207}Pb$) to provide independent age information and serve as a test for the extent to which closed system behavior has been adhered to after crystallization. Zircons are resistant to resetting caused by diagenetic alteration after deposition of the ash beds. We report 172 U/Pb zircon analyses from 10 ash beds from south China and one from Texas. A full discussion of error assessment and analytical details is given in (*17*) and (*18*), respectively.

Two samples were collected from the same ash bed from just above the base of the Changhsingian (MD96-7): the crystal-rich base (7b) and fine-grained top (7a). The zircons are euhedral, colorless, doubly terminated prisms (75 to 325 μm) that have aspect ratios that range from 8:1 to 1:1.5. Both opaque and clear inclusions of unknown composition are common. Twenty-three fractions of zircon were analyzed, and there is evidence for both an older component and lead loss. Twelve concordant analyses, including three single grains, define a cluster (Fig. 3A). The weighted mean $^{206}Pb/^{238}U$, $^{207}Pb/^{235}U$, and $^{207}Pb/^{206}Pb$ dates of this cluster of points are 253.4 ± 0.2 Ma [mean square weighted deviation (MSWD) = 1.46], 253.5 ± 0.2 Ma (MSWD = 0.85), and 254.4 ± 0.9 Ma (MSWD = 0.78), respectively. We interpret the age of MD96-7 to be 253.4 ± 0.2 Ma and regard this as the best estimate of the age of the basal Changhsingian.

The next highest dated horizon, MZ96-(−4.3), is 4.3 m below the white clay layer but not the biostratigraphic boundary, mid bed 27. This sample is a silicified tuff that weathers to a yellow to buff color. The zircons are euhedral, colorless, doubly terminated prisms (50 to 225 μm) that have aspect ratios that range from 5:1 to 1:1. Opaque and clear inclusions are ubiquitous. Fifteen fractions were analyzed. The weighted mean $^{206}Pb/^{238}U$, $^{207}Pb/^{235}U$, and $^{207}Pb/^{206}Pb$ dates of eight concordant fractions (including seven single grains) are 252.3 ± 0.3 Ma (MSWD = 0.95), 252.2 ± 0.4 Ma (MSWD = 0.34), and 251.8 ± 1.8 Ma (MSWD = 0.23), respectively (Fig. 3B). In this case, the $^{206}Pb/^{238}U$ age is more precise because of the small sample sizes and the less favorable ratios of radiogenic to common Pb. The best estimate of the age of this rock is 252.3 ± 0.3 Ma.

MAW-b25 is from a bentonite just below the paleontologically defined boundary at Meishan. Zircons separated from this unit have variable morphology and are euhedral, inclusion-rich, colorless, doubly terminated prisms (50 to 350 μm)

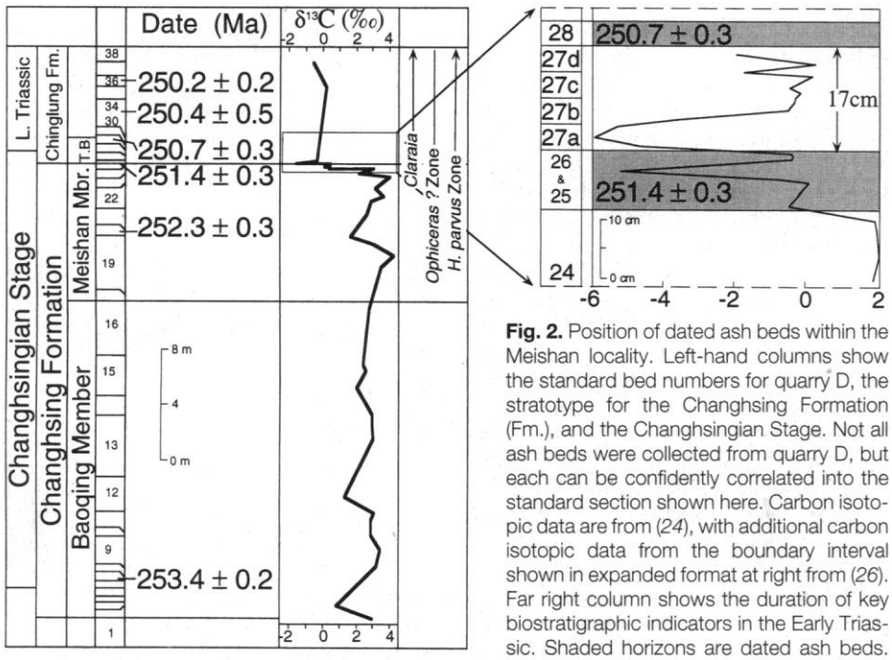

Fig. 2. Position of dated ash beds within the Meishan locality. Left-hand columns show the standard bed numbers for quarry D, the stratotype for the Changhsing Formation (Fm.), and the Changhsingian Stage. Not all ash beds were collected from quarry D, but each can be confidently correlated into the standard section shown here. Carbon isotopic data are from (*24*), with additional carbon isotopic data from the boundary interval shown in expanded format at right from (*26*). Far right column shows the duration of key biostratigraphic indicators in the Early Triassic. Shaded horizons are dated ash beds. T.B. signifies transitional beds with mixed Permian and Triassic fossils. Mbr., member.

with aspect ratios of 14:1 to 1:1. Twenty-four zircon fractions were analyzed from this sample, and the data define two statistically significant clusters on a concordia diagram (Fig. 3C). The upper cluster of five fractions is concordant and has weighted mean $^{206}Pb/^{238}U$, $^{207}Pb/^{235}U$, and $^{207}Pb/^{206}Pb$ dates of 252.7 ± 0.4 Ma (MSWD = 1.61), 252.8 ± 0.3 Ma (MSWD = 0.91), and 253.4 ± 3.0 Ma (MSWD = 1.12), respectively. The younger cluster is also concordant, and five points, including four single grains, yielded weighted mean $^{206}Pb/^{238}U$, $^{207}Pb/^{235}U$, and $^{207}Pb/^{206}Pb$ dates of 251.4 ± 0.3 Ma (MSWD = 0.37), 251.5 ± 0.5 Ma (MSWD = 0.02), and 253.6 ± 3.4 Ma (MSWD = 0.10), respectively. On the basis of our other dates from stratigraphically lower ashes, which are younger than 252.7 Ma, we regard the older cluster as a result of the inheritance of slightly older grains, perhaps incorporated during eruption. We interpret the younger cluster to be the best estimate of the age of the ash with an age of 251.4 ± 0.3 Ma.

Immediately above the boundary are three ashes: MZ96-(+0.17), MDB96-33, and MD96-293w, which correspond to beds 28, 33, and 36, respectively. Zircons separated from MZ96-(+0.17) are colorless, euhedral, inclusion-rich, doubly terminated prisms (50 to 225 μm) and have aspect ratios of 10:1 to 3:1. Nineteen fractions were analyzed and show evidence for both an older component and Pb loss. The age of the rock was estimated from nine concordant fractions, which define a cluster with weighted mean $^{206}Pb/^{238}U$, $^{207}Pb/^{235}U$, and $^{207}Pb/^{206}Pb$ dates of 250.7 ± 0.3 Ma (MSWD = 0.40), 250.6 ± 0.3 Ma (MSWD = 0.16), and 250.9 ± 3.3 Ma (MSWD = 0.66), respectively (Fig. 3D). The best estimate of the age of this rock is 250.7 ± 0.3 Ma.

Sample MDB96-33 is from a bentonite that yielded colorless, doubly terminated zircons (30 to 280 μm). Twelve fractions of zircon were analyzed and show both inheritance and Pb loss. A concordant cluster of seven analyses was used to calculate the weighted mean $^{206}Pb/^{238}U$, $^{207}Pb/^{235}U$, and $^{207}Pb/^{206}Pb$ dates of 250.4 ± 0.5 Ma (MSWD = 1.14), 250.7 ± 0.4 Ma (MSWD = 0.42), and 251.0 ± 7.5 Ma (MSWD = 1.85), respectively (Fig. 3E). The best estimate of the age of this volcanic layer is the weighted mean $^{206}Pb/^{238}U$ date of 250.4 ± 0.5 Ma, which is indistinguishable from that of MZ96-(+.17), which occurs stratigraphically just below.

Sample MD96-293w is of white bentonite that is locally up to 15 cm thick. Zircons

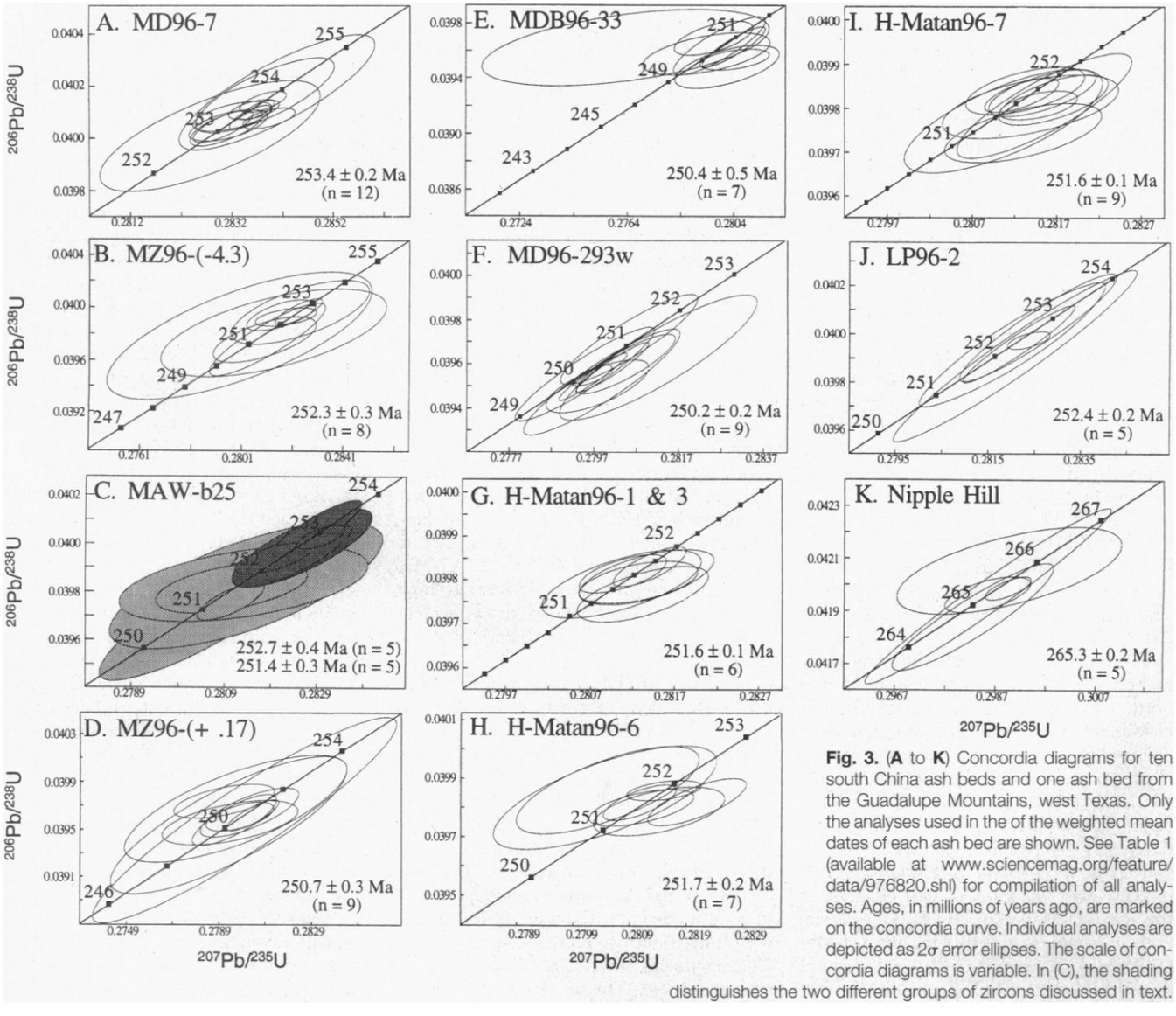

Fig. 3. (**A** to **K**) Concordia diagrams for ten south China ash beds and one ash bed from the Guadalupe Mountains, west Texas. Only the analyses used in the of the weighted mean dates of each ash bed are shown. See Table 1 (available at www.sciencemag.org/feature/data/976820.shl) for compilation of all analyses. Ages, in millions of years ago, are marked on the concordia curve. Individual analyses are depicted as 2σ error ellipses. The scale of concordia diagrams is variable. In (C), the shading distinguishes the two different groups of zircons discussed in text.

separated from it are euhedral, colorless, doubly terminated prisms (30 to 325 μm) that have aspect ratios of 8:1 to 1:1 and contain abundant inclusions. We analyzed 12 fractions. Nine concordant analyses yielded weighted mean $^{206}Pb/^{238}U$, $^{207}Pb/^{235}U$, and $^{207}Pb/^{206}Pb$ dates of 250.2 ± 0.2 Ma (MSWD = 0.57), 250.5 ± 0.2 Ma (MSWD = 0.47), and 253.7 ± 2.2 Ma (MSWD = 1.06), respectively (Fig. 3F). We interpret the best estimate of the age of this ash to be 250.2 ± 0.2 Ma.

The section at Heshan is characterized by a thick (10 m) sequence of volcanic rocks immediately below the boundary on both sides of the river (Fig. 1). The volcanic rocks comprise several cycles of thick-bedded crystal-rich tuffs that grade upward into clay-rich layers. We attribute these cycles to a proximal eruptive episode. We collected several samples to see if we could resolve small age differences within this unit and to test reproducibility.

The lowest samples, H-Matan96-1 and -3, were collected at the top and bottom of one graded sequence. They yielded a variety of zircons, many of them detrital. Twenty analyses were made, and many show evidence of inheritance or Pb loss. Six analyses from these two samples clustered about concordia and gave weighted mean $^{206}Pb/^{238}U$, $^{207}Pb/^{235}U$, and $^{207}Pb/^{206}Pb$ dates of 251.6 ± 0.1 Ma (MSWD = 0.60), 251.6 ± 0.1 Ma (MSWD = 0.18), and 252.1 ± 1.5 Ma (MSWD = 0.59), respectively (Fig. 3G). The best estimate of the age of this rock is 251.6 ± 0.1 Ma.

The highest sample, H-Matan96-6, is from just beneath the boundary on the south side of the river, where it is immediately overlain by the boundary sequence. Twelve fractions of zircon were analyzed, and seven were used to calculate the weighted mean $^{206}Pb/^{238}U$, $^{207}Pb/^{235}U$, and $^{207}Pb/^{206}Pb$ dates of 251.7 ± 0.2 Ma (MSWD = 0.75), 251.7 ± 0.3 Ma (MSWD = 0.80), and 251.4 ± 4.7 Ma (MSWD = 2.17), respectively (Fig. 3H). The best estimate of the age of this rock is 251.7 ± 0.2 Ma.

H-Matan96-7 is the stratigraphically highest exposure of volcanic ash on the north side of the river and correlates with H-Matan96-6. Sixteen zircon fractions were analyzed from this sample. A group of nine clustered about concordia and gave weighted mean $^{206}Pb/^{238}U$, $^{207}Pb/^{235}U$, and $^{207}Pb/^{206}Pb$ dates of 251.6 ± 0.1 Ma (MSWD = 0.87), 251.8 ± 0.1 Ma (MSWD = 0.17), and 252.9 ± 1.4 Ma (MSWD = 0.74), respectively (Fig. 3I). Our best estimate of the age of H-Matan96-7 is 251.6 ± 0.1 Ma.

Four samples from this locality (H-Matan96-1, -3, -6, and -7) yielded ages that are statistically identical (251.6 ± 0.1, 251.7 ± 0.2, and 251.6 ± 0.1 Ma, respectively). These results demonstrate that our ages are very reproducible and that the calculated uncertainties accurately describe all sources of nonsystematic error.

Sample LP96-2 from Penglaitan contains abundant zircons, some of which are detrital, as well as small grains of monazite. It is unclear whether the monazites are primary phenocrysts or formed by diagenesis. The monazite is rich in Th and has high common Pb content, which precludes precise U/Pb age determination. Twelve fractions of zircon were analyzed and five clustered around concordia and gave weighted mean $^{206}Pb/^{238}U$, $^{207}Pb/^{235}U$, and $^{207}Pb/^{206}Pb$ dates of 252.4 ± 0.2 Ma (MSWD = 0.10), 252.6 ± 0.4 Ma (MSWD = 0.06), and 253.6 ± 1.7 Ma (MSWD = 0.21), respectively (Fig. 3J). We interpret the age of LP96-2 to be 252.4 ± 0.2 Ma. This sample is from within the late Changhsingian Stage, but its exact location relative to the conodont zonation is uncertain.

Six zircon fractions analyzed from the ash exposed on Nipple Hill define a concordant cluster of data. Five fractions from this sample yielded weighted mean $^{206}Pb/^{238}U$, $^{207}Pb/^{235}U$, and $^{207}Pb/^{206}Pb$ dates of 265.3 ± 0.2 Ma (MSWD = 0.50), 265.4 ± 0.3 Ma (MSWD = 0.25), and 266.5 ± 1.8 Ma (MSWD = 0.25), respectively (Fig. 3K). The best estimate of the age of this ash is 265.3 ± 0.2 Ma, which provides a maximum estimate for the age of the base of the Capitanian.

Implications of geochronology for understanding the mechanisms of extinction. Our data have several implications for understanding mechanisms that contributed to the biological and chemical events associated with the end-Permian mass extinction. At Meishan, the age of the event boundary is 251.4 ± 0.3 Ma, and the biostratigraphically defined P-T boundary is <251.4 ± 0.3 Ma and >250.7 ± 0.3 Ma. The age data from the Heshan section show that the age of the boundary in two widely separated localities (~1500 km) is about the same.

Within south China, the major pulse of the end-Permian extinction is confined largely to the upper member of the Changhsingian Stage. Diverse marine assemblages of brachiopods, bivalves, conodonts, ammonoids, and other taxa occur throughout south China in the C. *subcarinata* zone of the lower Changhsingian and persist into the overlying unit. The youngest Permian reefs are in the *Paleofusulina sinensis* fusulinid zone in Sichaun Province (*19*) but not within the final two conodont zones of the Changhsingian (the C. *yingi* and C. *meishanensis* zones). Throughout south China, 280 of 329 genera (85%) of marine invertebrates became extinct within the C. *changhsingensis* and C. *yingi* conodont zones (equivalent to the *P. sinensis* fusulinid zone) of the upper stage and thus largely above MZ96-(−4.3) (bed 20). These genera include all fusulinid forams and corals, 85% of articulate brachiopod genera, 94% of nonfusulinid forams, 97% of ammonoids, 85% of gastropods, and 59% of bivalves (*20*). At Meishan, most last appearances occur within 50 cm of the boundary, between units 24c and 24d (*20*). Correlations with conodonts and the carbon isotopic excursion suggest that the extinction was equally rapid in Spitsbergen (*21*) and the Alps (*22*). Further detailed studies, including statistical analysis of range end points, are required to analyze the pattern of extinction (*23*) and the relation between the disappearances, the ash beds, and the isotopic excursion. Our geochronological data indicate that the main pulse of Changhsingian extinction occurred in less than 1 My (between 251.4 ± 0.3 and 252.3 ± 0.3 Ma).

At Meishan as well as at other sections, there are abrupt negative shifts in the $\delta^{13}C$ value of carbonates (both inorganic and organic carbon) at the P-T boundary (*21*, *24*–*27*). The amplitude and wavelength of the shifts are a function of accumulation rate and sampling interval. In many studies, a shift from the Late Permian to the Early Triassic values of −2 to −4 per mil is observed with the maximum excursion approximately coinciding with the boundary (*24*, *25*) At Meshian, detailed sampling shows that there is an abrupt negative excursion in $\delta^{13}C$ to as low as −6 per mil above the "boundary ash" and close to the biostratigraphically defined boundary (*20*, *26*) (unit 27c, Fig. 2). This sharp spike is mostly within the 4- to 5-cm-thick unit 27a, although a single very negative sample was recorded from bed 26. The $\delta^{13}C$ value recovered to 0 per mil by the first occurrence of *H. parvus* at the base of bed 27c.

Our geochronological data limit the maximum duration of the isotopic excursion. The main high-amplitude excursion to −6 per mil takes place within unit 27a (4 cm). Accumulation rates for bed 27 can be estimated with the ages of ash beds 25 and 28 and yield a duration for the spike of less than 165,000 years (*28*). This result implies that there was a catastrophic input of isotopically light carbon to the oceans. Until detailed (centimeter scale) sampling is done in other sections, it is difficult to evaluate whether this short duration spike is unique to Meishan.

Proposed hypotheses to explain the end-Permian extinction include the following: effects from a bolide impact (*29*) or flood basalt volcanism (*12*, *30*), overturn of a

stratified ocean and poisoning of shelf areas with CO_2-rich waters (6, *31*, *32*), transgression-associated anoxia (8), and a variety of environmental effects associated with a major marine regression (*1*, *2*). Any hypothesis must explain the short duration (<1 My) of the final pulse of extinction.

The age of the Siberian flood basalt volcanism has been reported to be identical within error to that of the P-T boundary at Meishan and to have a duration of 1 My or less as indicated by $^{40}Ar/^{39}Ar$ and U/Pb dates (*12*, *33*, *34*). Direct comparison of $^{40}Ar/^{39}Ar$ and U/Pb ages is difficult because of possible interlaboratory biases in the Ar standards and uncertainty in the decay constants (*35*). A U/Pb zircon and badellyite age for the Noril'sk-1 gabbroic intrusion, which cuts the lower third of the Siberian Traps, is 251.2 ± 0.3 Ma (*34*). Renne *et al.* (*35*) indicate that recalculation of previously reported Ar data (*12*) yields an age of 250.0 ± 4.6 Ma (2σ; including all systematic uncertainties affecting the $^{40}Ar/^{39}Ar$ system) for the initiation of Siberian Trap volcanism (including biotite from the Noril'sk-1 intrusion). Comparison of the $^{40}Ar/^{39}Ar$ ages of the traps with the $^{40}Ar/^{39}Ar$ age of the P-T boundary may be done without considering systematic errors, leading to the conclusion that the two were synchronous within <360,000 years (*12*). Our best estimate for the age of the boundary is <251.4 and >250.7 Ma, and thus the U/Pb ages for the two events coincide.

However, in our opinion, for the eruption of the Siberian Traps to be considered a cause of extinction, it should predate the onset of the extinction. Our data indicate that most of the Changhsingian extinction occurred between 252.3 and 251.4 Ma. If the traps were involved, eruption would had to have begun before 252 Ma, which is permitted by the U/Pb data (*33*). $^{40}Ar/^{39}Ar$ dating in the nearby Meimecha-Kotui subprovince indicates that precursory volcanism began at 253.3 ± 2.6 Ma (*36*), supporting the expected relative timing of cause and effect. On the other hand, an earliest Triassic eruption of the Siberian Traps is also consistent with the data, with the environmental effects of the eruptions perhaps having been responsible for retarding the biotic recovery but not having been involved in the extinction itself. However, the overall eruptive history of the Siberian Traps remains incompletely known.

Despite the possible temporal coincidence of Siberian Trap volcanism and the P-T boundary, a causal connection remains unclear. Visscher *et al.* (*30*) have suggested that the destruction of terrestrial ecosystems was recorded by the late Changhsingian increase in the abundance of fungal spores that reflect acid rain from sulfate aerosols associated with volcanism. Suggestions that sulfate aerosols generated acid rain are plausible and are consistent with the destruction of both marine and terrestrial ecosystems, although it is not clear that this model is consistent with the pattern of selective marine extinction. How much sulfate aerosol or carbon dioxide was released is poorly constrained. Because volcanic carbon is not sufficiently light to produce the observed $\delta^{13}C$ shift, given the assumption of reasonable volumes (*1*), the eruption of the Siberian Traps is at best only a partial explanation of the observations.

The $\delta^{13}C$ isotopic shift is approximately coincident with the maximum pulse of extinction in the latest Changhsingian and with the eruption of the Siberian Traps. Most discussions of the isotopic shift have focused on causes affecting the whole ocean, including the following: (i) exposure of marine organic carbon (*27*) or gas hydrates (*1*) in continental shelves associated with a major regression; (ii) marine anoxia associated with oxidation of isotopically depleted, CO_2-enriched bottom waters during rapid overturn (6, *32*); (iii) onshore migration of a dysaerobic layer during transgression (8); (iv) collapse of surface to deep $\delta^{13}C$ gradient due to the extinction and its aftermath, which resulted in the export of less isotopically light carbon to the deep ocean (*37*–39) and a shift of whole-ocean values to more negative values (the magnitude of the shift would depend on how much organic carbon burial continued on the shelves); and (v) oxidation of Late Permian peat deposits (*40*).

Erosional unconformities throughout south China and elsewhere suggest that there was a minor regression near the P-T boundary, but estimates of a sea level drop of more than 200 m (*41*) are unsubstantiated (*5*, *8*, *20*). Detailed stratigraphic analysis reveals a maximum low stand near the Wuchaipingian-Changhsingian boundary (*5*, *20*) or during the lower Changhsingian (*8*). Our geochronological data from Meishan (Fig. 2), however, indicate that the sediment accumulation rate increased across the boundary consistent with transgression. The timing of the isotopic shift and lack of evidence for a major erosional unconformity make a major episode of regression (exposing organic carbon or releasing gas hydrates) followed by a major transgression (flooding the shelves with isotopically light carbon) unlikely. Although gas hydrates are an ideal source for driving the isotopic shift (*1*), the lack of evidence for a major regression and the observation that the latest Permian was a time of a global sea level low stand rule out this scenario. The short-lived excursion (<165,000 years) of $\delta^{13}C$ values to −6 per mil as reported by Xu and Yan (*26*) at the boundary at Meishan can most easily be driven by sudden release of isotopically light carbon such as methane or oxidation of organic carbon.

Although oceanic overturn remains a plausible mechanism, there is no geological evidence (glacial deposits) to support glacially induced overturn, as suggested by Knoll *et al.* (6). The deep-sea record (*31*) of long-term deep-water anoxia from Late Permian through Early Triassic exhibits little indication of a major "event" at the boundary, which is inconsistent with a catastrophic overturn of the oceans. Onshore movement of a dysaerobic layer (8) appears insufficient because the dysaerobic layer would require a minimum of 3000 gigatons (Gt) of carbon to cause the observed isotopic shift. In addition, persistence of shallow water marine anoxia requires greatly reduced atmospheric oxygen concentrations.

On the other hand, the isotopic excursion might not reflect a whole-ocean shift in the carbon cycle. A whole-ocean $\delta^{13}C$ shift from +2 to 0 per mil (average Late Permian values to average earliest Triassic values) coupled with a transient surface-ocean shift of −1 to −2 per mil (39) through collapse in primary productivity is also plausible. The volume of carbon required to drive this shift (*1*, *42*) drops correspondingly, depending on the source and thus the $\delta^{13}C$ value of the carbon (*43*). In this scenario, the extinction and drop in primary productivity are related, and the extinction causes the isotopic shift. The whole-ocean shift of +2 to 0 per mil could also have resulted from the collapse of primary productivity or ecosystem structuring if the collapse caused a decrease in organic burial rates.

The isotopic shift and perhaps the final extinction could also be related to a bolide impact (*29*, *44*–*46*). The brief negative excursion and the abrupt change in climate could be due to rapid delivery of isotopically light carbon in the form of CO_2 or methane (or both) (*47*, *48*). Impact of a comet or icy body with Earth's atmosphere would unleash a sequence of chemical reactions (*46*, *49*) but, because of its volatile nature, leave little trace. An icy, carbon-rich comet would be rapidly converted to CO_2 in our oxygen-rich atmosphere, resulting in acid rain and greenhouse warming. Acid rain is predicted to lower shallow marine pH to depths of at least 150 m such that carbonates would dissolve and release large amounts of CO_2 (*49*). Similar effects would be expected if the object contained large amounts of nitrogen-bearing compounds. Methane could also be released from shock heating of gas hydrates. If it survived atmospheric disintegration and impacted the oceans, a body of sufficient size (>10 km)

could mix a large volume of the oceans (*32*, *46*); the persistence of deep-water anoxia through the boundary (*8*, *31*), however, suggests that no such perturbation occurred.

The following seven observations must be accommodated in any model for the P-T extinction: (i) the widespread evidence of anoxia in latest Permian–earliest Triassic deep-ocean sediments (*31*), including accumulation of massive amounts of organic carbon (*50*); (ii) the $\delta^{13}C$ isotopic excursion at or near the P-T boundary in both marine and terrestrial ecosystems, although the precise relation between peak extinction and the isotopic shift remains unclear; (iii) evidence for anoxia in nearshore settings at or close to the P-T boundary (*8*), coincident with a major earliest Triassic transgression (*41*); (iv) patterns of extinction consistent with hypocapnia or CO_2 poisoning (6); (v) the age of the Siberian Traps and extinction being the same within error; (vi) a lack of evidence for a latest Permian glaciation (*1*); and (vii) sudden climate warming at and after the boundary (*51*).

On the basis of our high-precision geochronology, we suggest three possible scenarios to explain the events at the P-T boundary. In the first, eruption of the Siberian flood basalts in the latest Changhsingian released large amounts of CO_2 (and possibly sulfates, producing acid rain) and initiated a period of global warming. Warming of shallow seas lowered the lysocline sufficiently to release some 1200 Gt of oceanic methane hydrates (*52*). Following the scenario of Renne *et al.* (*12*), a short volcanic winter triggered by volcanic aerosols was followed by greenhouse conditions and warming. This cooling-warming cycle could have triggered convective overturn of the oceans, dumping deep CO_2-rich bottom water onto the shelf regions (6), leading to hypocapnia and increased atmospheric CO_2.

In the second scenario, extinction, perhaps related to the Siberian Traps, eliminated primary productivity and export of light carbon to the deep ocean, which produced a transient isotopic shift; the oceans returned $\delta^{13}C$ values of around 0 per mil during recovery. It is possible that the export of sequestered light carbon and CO_2 charged water by upwelling, combined with volcanic eruption–induced extinction, could explain the observations. No single mechanism is sufficient to explain all the geological and paleontological data in either of these scenarios, but the massive eruption of the Siberian Traps may well have been the proximal cause for a cascade of events leading to the apparent synchroneity of marine and terrestrial extinctions.

The final possibility is that the latest Permian biota was already in decline as a result of the above scenarios and that the collision of Earth and an icy object was the final catalyst that pushed the planet to the brink of total extinction. A carbon-rich bolide 10 km or greater in diameter could have delivered or caused a massive infusion of CO_2 to the atmosphere and oceans that was the trigger for the final and most profound pulse of extinction at the boundary. Massive volcanism, both marine and continental, acid rain, anoxia, and the other mechanisms discussed above have been operative at other times in Earth history and may have played a role in other less dramatic extinctions. However, the annihilation of 70 to 90% of all species is truly a singular event in Earth history and may require such an explanation.

Geochronology of the P-T boundary section in southern China now outstrips the available paleontological and chemostratigraphic resolution. The geochronological data presented here allow specific tests of extinction scenarios and the ability to focus on outstanding problems with a precise chronological framework. The rapidity of the extinction and its synchroneity with the rapid $\delta^{13}C$ isotopic excursion and the eruption of the Siberian Traps are no longer in doubt. The distribution of dated ash beds at Meishan allows estimates of the distribution of time at better than the 50,000-year level. Outstanding issues and questions are as follows: (i) Although we have shown that the age of the boundary is about the same in two widely separated localities in south China, it remains to be documented whether the boundary has exactly the same age across all of Pangea. (ii) Did the extinction occur at exactly the same time in terrestrial and marine environments? (iii) Is the $\delta^{13}C$ shift the result of the extinction (collapse of primary productivity), the signature of upwelling of deep CO_2-charged bottom water, the result of a cometary impact, or a combination thereof? (iv) A detailed comparison of carbon isotope variations with the extinction chronology is necessary to better evaluate a relation. (v) After its demise in <1 My, how quickly did life rebound during the earliest Triassic?

REFERENCES AND NOTES

1. D. H. Erwin, *The Great Paleozoic Crisis* (Cambridge Univ. Press, New York, 1993).
2. ———, *Nature* **367**, 231 (1994).
3. C. C. Labandeira and J. J. Sepkoski Jr., *Science* **261**, 310 (1993).
4. S. M. Stanley and X. Yang, *ibid.* **266**, 1340 (1994).
5. Y. G. Jin, J. Zhang, Q. H. Shang, *Can. Soc. Pet. Geol. Mem.* **17**, 813 (1994).
6. A. H. Knoll, R. K. Bambach, D. E. Canfield, J. P. Grotzinger, *Science* **273**, 452 (1996).
7. D. H. Erwin, in *Evolutionary Paleobiology*, D. Jablonski, D. H. Erwin, J. H. Lipps, Eds. (Univ. of Chicago Press, Chicago, IL, 1996), pp. 398–418.
8. P. B. Wignall and A. Hallam, *Palaeogeogr. Palaeoclimatol. Palaeoecol.* **93**, 21 (1992); *ibid.* **102**, 215 (1993); *Palaios* **11**, 587 (1996); P. B. Wignall and R. J. Twitchett, *Science* **272**, 1155 (1996); P. B. Wignall, H. Kozur, A. Hallam, *Hist. Biol.* **12**, 39 (1996).
9. Z. Y. Yang, J. Z. Sheng, H. F. Yin, *Episodes* **18**, 49 (1995); H. F. Yin, *Paleoworld* **4**, 153 (1994); S. L. Mei, K. Zhang, B. R. Wardlaw, *Palaeogeogr. Palaeoclimatol. Palaeoecol.*, in press. In the official time scale for the Permian System approved recently by the Subcommission on the Permian Stratigraphy, International Union of Geological Sciences [Y. G. Jin, B. Wardlaw, B. F. Glenister, C. V. Kotlyar, *Episodes* **20**, 10 (1997)], the Middle and the Late Permian are typified by the Guadalupian Series in the southwestern United States and the Lopingian Series in south China, respectively. The latter is subdivided into the Wuchiapingian Stage in the lower and the Changhsingian Stage in the upper.
10. Z. Zichao, *Bull. Liais. Inform. IUGS Subcomm. Geochronol.* **B10**, 14 (1992).
11. J. C. Claoue-Long, Z. C. Zhang, G. G. Ma, S. H. Du, *Earth Planet. Sci. Lett.* **105**, 182 (1991).
12. P. R. Renne, Z. Zichao, M. A. Richards, M. T. Black, and A. R. Basu [*Science* **269**, 1413 (1995)] note that the P-T boundary is 5 cm above the sampled bentonite on the basis of an older position of the boundary. The position of the paleontologically defined P-T boundary is currently within bed 27c and thus above the bentonite at beds 25 and 26.
13. M. Menning, in *The Permian of Northern Pangea*, P. A. Scholle, T. M. Peryt, D. S. Ulmer-Scholle, Eds. (Springer-Verlag, Berlin, Germany, 1995), vol. 1, pp. 77–97.
14. J. Roberts, J. C. Claoue-Long, C. B. Foster, *Aust. J. Earth Sci.* **43**, 401 (1996).
15. V. Palmieri, C. B. Foster, E. V. Bondareva, *AGSO J. Aust. Geol. Geophys.* **15**, 359 (1994).
16. B. F. Glennister *et al.*, *Int. Geol. Rev.* **34**, 857 (1992).
17. The sources of error in individual U/Pb isotopic age determinations have been well described (*53*) and include the following: precision and accuracy of isotopic measurements that are largely related to nonlinear response of amplifier gains, counting statistics on low-abundance Pb isotopes (^{204}Pb), uncertainty in mass-dependent fractionation, the amount and composition of analytical blank for each analysis, and the ratio of radiogenic to common Pb. In general, the uncertainties associated with making blank and common Pb corrections can be minimized with large radiogenic Pb/common Pb ratios, which generally scale with sample size. Sources of systematic error may include errors in spike calibration and uncertainty in the decay constants for U. These uncertainties would apply to all analyses done in a particular lab; although they might affect absolute age determinations, the relative age differences between beds are not affected. Resolution of time at the ±300,000-year time frame for Permian-aged volcanic rocks provides a special set of problems. The most substantial problem is one's ability to distinguish small amounts of Pb loss or inheritance (or both). It is common in air fall ash deposits to find zircon grains, probably incorporated into the eruption column, that are identical in morphology to the indigenous population but that can be <1 to >10 My older (*54*). This problem can be minimized by dating single grains of zircon with high concentrations of Pb. In this way, the uncertainty on all three dates ($^{206}Pb/^{238}U$, $^{207}Pb/^{235}U$, and $^{207}Pb/^{206}Pb$) is low (0.1 to 0.3%), and the difference between the $^{206}Pb/^{238}U$ and $^{207}Pb/^{235}U$ dates can be evaluated for inheritance or Pb loss (or both). Although it is possible to analyze as little as 5 to 10 pg of radiogenic Pb, doing so for zircon with high common Pb is problematic; if the total common Pb (blank plus sample) is such that the radiogenic to common ratio is less than 5, the uncertainties on the $^{207}Pb/^{235}U$ and $^{207}Pb/^{206}Pb$ age become large because of the low abundance of radiogenic ^{207}Pb relative to ^{206}Pb. Thus, there is a trade-off between sample size and uncertainty. It is this limitation that requires SHRIMP to use only the $^{206}Pb/^{238}U$ date when determining the age of Paleozoic zircons and why conventional isotope dilution thermal ionization mass spectrometry analyses on ultrasmall samples or

those with low radiogenic/common ratios depend on the $^{206}Pb/^{238}U$ dates for calculating the age of a rock (*55*). The zircons we studied contained as little as 3 pg of radiogenic Pb per grain, and the amount of Pb analyzed in each fraction (excluding inherited grains) typically ranged from 10 to 60 pg. Analytical blanks varied from 0.65 to 3.5 pg. In many cases, we analyzed both multigrain and single-grain fractions. The $^{206}Pb/^{238}U$ and $^{207}Pb/^{235}U$ dates are sufficiently precise to evaluate concordance in some cases. To calculate the age of the ash bed, we used the weighted mean of the $^{206}Pb/^{238}U$ and $^{207}Pb/^{235}U$ dates from concordant analyses. When displayed graphically (Fig. 3), the data tend to cluster about the concordia curve. Analyses that fall below the cluster were interpreted as discordant because of Pb loss, and those that plot to the right and above the cluster were interpreted as containing an older component. Except for one sample, we analyzed a minimum of 12 fractions per sample. The weighted mean age reported for each of the ash beds in this paper is quoted at the 95% confidence interval. In many cases, the weighted mean $^{207}Pb/^{235}U$ date has a lower MSWD and higher uncertainty than the $^{206}Pb/^{238}U$ date. This is because there is substantially less ^{207}Pb than ^{206}Pb, and thus the common Pb correction has a much larger effect on the $^{207}Pb/^{235}U$ date and the corresponding errors are larger, making it more likely that the excess scatter in the weighted mean is not resolved from analytical error. We selected a statistically significant cluster of analyses and then calculated the weighted mean $^{206}Pb/^{238}U$ and $^{207}Pb/^{235}U$ dates. The best estimate for the age of the zircons can be either the average of the two U/Pb dates (if the uncertainties are comparable) or the weighted mean of the $^{206}Pb/^{238}U$ dates, which is always the most precise. Some analyses are concordant but are distinctly older or younger than the cluster used to calculate the weighted means. Selection of the analyses to use in the weighted mean calculation is necessarily somewhat subjective. Analyses with large uncertainties (>2%), for example, are often not used nor are ones that fall out of the main cluster. It is only with a large number of analyses per sample and the stratigraphic context of a sequence containing several ash beds that we can confidently calculate the best estimate of the age of a particular sample. The high degree of reproducibility shown by the four samples from H-Matan confirms that our approach is successful. In samples with total common Pb concentrations greater than the 3.5 pg, we assumed that the additional common Pb was incorporated into the zircons as inclusions [glass, fluid, or sulfide(?)]. If the assigned blank concentration was too low [samples with high total common Pb (up to 10 pg)], which may reflect laboratory contamination and not indigenous common Pb, then the uncertainties were underestimated. For total common Pb values less than 3.5 pg, we assumed that all of the common Pb was blank.

18. Zircons were separated from the samples with standard techniques of crushing, Wilfley table, magnetic separation, and heavy liquids for silicified samples. Bentonites were soaked in a mixture of water and soap, and the clay fraction was decanted off before magnetic and heavy liquid separation. Zircons were selected on the basis of size, color, and the lack of inclusions and then air abraded (*56*) to remove the outer portion of the grains and acid washed in warm 4 M HNO_3 for several hours before dissolution in HF + HNO_3. The zircons were spiked with a mixed ^{205}Pb-^{233}U-^{235}U tracer solution before dissolution in Teflon microcapsules at 220°C for 48 hours. Pb and U were separated from the resulting solution with anion exchange chemistry adapted after Krogh (*57*). Total analytical blanks were 0.65 to 3.5 pg for Pb and less than 1.0 pg for U. Total common Pb is reported for each analysis in Table 1 (available at www.sciencemag.org/feature/data/976820.shl). Pb was loaded on single rhenium filaments with silica gel and phosphoric acid. Isotopes of Pb were measured with a VG Sector-54 thermal ionization mass spectrometer with a Daly detector in ion-counting mode. In general, an ion beam between 0.2 and 0.8 × 10^{-13} A was maintained for ^{206}Pb during data acquisition. Uranium was loaded with phosphoric acid and colloidal graphite on rhenium filaments and was measured as metal ions in static mode with three Faraday collectors and an average ^{235}U ion beam intensity of 2.5 × 10^{-13} A. Errors in the $^{206}U/^{238}Pb$, $^{207}U/^{235}Pb$, and $^{207}Pb/^{206}Pb$ ages were estimated with the methods of Ludwig (*58*), and all age uncertainties are quoted at the 95% confidence level. Data acquired with the Daly detector were corrected only for fractionation based on replicate runs of NBS 981 common Pb standard. Additional analytical details are presented in Table 1 (available at www.sciencemag.org/feature/data/976820.shl).
19. J. W. Reinhardt, *Facies* **18**, 231 (1988).
20. Ammonoid data are from Z. Zhou, B. F. Glennister, W. M. Furnish, and C. Spinosa [*Permophiles* **29**, 52 (1996)], gastropod data are from D. H. Erwin (unpublished data), and brachiopod data are from S. Z. Shen and G. R. Shi [*Hist. Biol.* **12**, 93 (1996)]. Other data are from Z. Y. Yang *et al.* [*Permo-Triassic Events of South China* (Geological Publishing House, Beijing, 1993)].
21. P. B. Wignall, R. Morante, R. Newton, *Geol. Mag.* **135**, 47 (1997).
22. C. Broglio-Lorgia and G. Cassinis, in *Permo-Triassic Events in the Eastern Tethys*, W. C. Sweet, Z. Y. Yang, J. M. Dickins, H. F. Yin, Eds. (Cambridge Univ. Press, Cambridge, 1992), pp. 78–98.
23. C. R. Marshall and P. D. Ward, *Science* **274**, 1360 (1996).
24. A. Baud, M. Magaritz, W. T. Holser, *Geol. Rundsch.* **78**, 649 (1989).
25. Several different numbering schemes have been applied to the beds in the Meishan section, reflecting progressive refinement of the stratigraphy; we follow that currently used by the Nanjing Institute. Beds 25 and 26 of this paper correspond to beds 22 and 23 of (*24*).
26. D. U. Xu and Z. Yan, *Palaeogeogr. Palaeoclimatol. Palaeoecol.* **104**, 171 (1993). No analytical details are given in this paper.
27. W. T. Holser and H. P. Schonlaub, *Abh. Geol. Bundesanst.* **45**, 1 (1991).
28. Field evidence suggests a hiatus at the top of bed 25 that would shorten the duration of the isotopic shift. Accumulation rates between MZ96-(−4.3) and MD96-293w are much higher (1 cm per 2000 years), which would yield a duration of less than 10,000 years for the isotopic excursion. Alternatively, if a substantial amount of time is missing at the top of bed 25, only part of the spike may be preserved.
29. D. Y. Xu *et al.*, *Nature* **314**, 154 (1985); G. J. Retallack, A. Seyedolai, W. T. Holser, D. Krinsley, E. S. Krull, *Geol. Soc. Am. Abstr. Program* **28**, A-368 (1996).
30. H. Visscher *et al.*, *Proc. Natl. Acad. Sci. U.S.A.* **93**, 2155 (1996).
31. Y. Isozaki, *Science* **276**, 235 (1997).
32. Y. Kajiwara, S. Yamakita, K. Ishida, H. Ishiga, A. Imai, *Palaeogeogr. Palaeoclimatol. Palaeoecol.* **111**, 367 (1993).
33. I. H. Campbell, G. K. Czamanske, V. A. Fedorenko, R. I. Hill, V. Stepanov, *Science* **258**, 1760 (1992); P. R. Renne and A. R. Basu, *ibid.* **253**, 176 (1991).
34. S. L. Kamo, G. K. Czamanske, T. E. Krogh, *Geochim. Cosmochim. Acta* **60**, 3505 (1996).
35. P. R. Renne *et al.*, *Chem. Geol. Isot. Geosci. Sect.* **145**, 117 (1998).
36. A. R. Basu *et al.*, *Science* **269**, 822 (1995).
37. S. D'Hondt and P. Donaghay, *Geol. Soc. Am. Abstr. Program* **27**, A-164 (1995).
38. K. Wang, H. H. Geldsetzer, H. R. Krouse, *Geology* **22**, 580 (1994).
39. W. T. Holser, *30th Int. Geol. Cong. Abstr.* **2**, 58 (1996).
40. K. Faure, M. J. de Wit, J. P. Willis, *Geology* **23**, 507 (1995).
41. W. T. Holser and M. Magaritz, *Mod. Geol.* **11**, 155 (1987).
42. A. Spitzy and E. T. Degans, *Mitt. Geol.-Palaontol. Inst. Univ. Hamburg* **59**, 155 (1985).
43. With the assumption of a value of 40,000 Gt of dissolved inorganic carbon (the value for the present ocean), a whole-ocean shift from +3 to +1 per mil would require 13,000 Gt at −5 per mil, 3700 to 3000 Gt of marine organic carbon at −20 to −25 per mil, and 1100 Gt of methane gas hydrates at −65 per mil. The corresponding values for a shift from +3 to 0 per mil are 24,000 Gt, 5800 to 4700 Gt, and 1700 Gt. However, isotopic evidence suggests that Late Permian oceans contained a much larger volume of dissolved inorganic carbon, which would increase the above estimates. If Permian oceans contained 60,000 Gt of dissolved inorganic carbon, for example, all of the above estimates would be increased by one-third.
44. D. J. McLaren and W. D. Goodfellow, *Annu. Rev. Earth Planet. Sci.* **18**, 123 (1990).
45. M. R. Rampino and B. M. Haggerty, *Geol. Soc. Am. Spec. Pap.* **307**, 11 (1996).
46. P. Wilde and M. S. Quimby-Hunt, *Palaeogeogr. Palaeoclimatol. Palaeoecol.* **132**, 47 (1997).
47. D. C. Jewitt, H. E. Matthews, T. Owen, R. Meier, *Science* **278**, 90 (1997).
48. Recent estimates of the carbon isotopic composition of Comet C/1995 O1 (Hale-Bopp) indicate carbon much lighter than the solar system average or even methane (*47*). Thus, it is possible that a carbon-rich bolide could cause a negative isotopic shift.
49. R. G. Prinn and B. Fegley Jr., *Earth Planet Sci. Lett.* **83**, 1 (1987).
50. Y. Isozaki, *Geol. Soc. Am. Abstr. Program* **29**, 339 (1997).
51. K. G. MacLeod, *Geol. Soc. Am. Abstr. Program* **29**, 462 (1997); G. J. Retallack, *Aust. J. Earth Sci.* **44**, 185 (1997).
52. G. R. Dickens, M. M. Castillo, J. C. G. Walker, *Geology* **25**, 259 (1997).
53. K. R. Ludwig, *Earth Planet. Sci. Lett.* **46**, 212 (1980).
54. E. Landing *et al.*, *Can. J. Earth Sci.*, in press.
55. R. Mundil, P. Brack, M. Meier, H. Rieber, and F. Oberli, *Earth Planet Sci. Lett.* **141**, 137 (1996).
56. T. E. Krogh, *Geochim. Cosmochim. Acta* **37**, 488 (1973).
57. ———, *ibid.* **46**, 637 (1982).
58. K. R. Ludwig, *U.S. Geol. Surv. Open File Rep. 88-557* (1988).
59. We thank NASA, the Smithsonian Institution, the Academia Sinica, and National Natural Science Foundation, China for support. Access to Guadalupe Mountains National Park was provided by L. Henderson and F. A. Armstrong. D. Coleman took part in the sampling of ash beds in China in 1996 and is thanked for his enthusiastic participation. Reviews by two anonymous referees and P. Enos improved the manuscript, as did discussions with P. Renne, S. D'Hondt, J. Grotzinger, and B. Wardlaw.

19 December 1997; accepted 12 March 1998